Array 30 (2026) 100961

Contents lists available at ScienceDirect

Array

journal homepage: www.elsevier.com/locate/array

RatioWaveNet: A learnable wavelet-based framework for robust and interpretable electroencephalogram motor imagery classification

Marco Siino *, Giuseppe Bonomo, Rosario Sorbello, Ilenia Tinnirello

University of Palermo, Italy

ARTICLE INFO

Keywords:
Electroencephalogram decoding
Rational Dilated Wavelet Transform
Temporal convolutional networks
Attention mechanisms
Brain–computer interfaces
Neural signal processing

ABSTRACT

Decoding non-stationary electroencephalogram (EEG) signals remains a primary bottleneck in developing reliable Brain–Computer Interfaces (BCIs). Traditional deep learning approaches often struggle with complex spatiotemporal dynamics, low signal-to-noise ratios, and severe inter-subject variability. To address these challenges, we propose RatioWaveNet, a novel deep learning framework that integrates a Rational Dilated Wavelet Transform (RDWT) with a hybrid multi-window attention and Temporal Convolutional Network (TCN) architecture. Unlike conventional fixed-dilation transforms, our approach leverages learnable rational dilation factors to dynamically optimize time–frequency resolution for specific motor imagery rhythms. The pipeline combines dilated convolutional layers for spatial filtering, a multi-window mechanism merging multi-head and convolutional block attention for spatiotemporal dependency modeling, and a hierarchical TCN for sequential decoding. Comprehensive experiments across three public EEG benchmarks demonstrate that RatioWaveNet achieves statistically significant performance gains, yielding a 3%–7% accuracy improvement ($p < 0.01$) over current state-of-the-art methods. Furthermore, rigorous cross-subject evaluations confirm enhanced model robustness and stable decision-making under severe subject shifts. Beyond raw accuracy improvements, RatioWaveNet offers a highly interpretable and mathematically grounded framework. The RDWT front-end provides physiologically meaningful feature representations — corroborated by scalogram visualizations — while the attention-TCN core ensures noise-resilient decoding. These advancements establish RatioWaveNet as a highly effective and transparent solution for high-fidelity EEG classification. The complete codebase and pretrained models are publicly released to promote reproducibility.

1. Introduction

Decoding electroencephalographic (EEG) signals for Brain-Computer Interfaces (BCIs) remains a challenging problem due to the signals' inherent non-stationarity [1,2], low signal-to-noise ratio [3,4], and significant inter-subject variability [5,6]. EEG signals are additionally affected by emotional and physiological states of the subject [7,8], which often introduce further noise and artifacts that degrade decoding accuracy. Consequently, robust noise suppression and adaptive feature extraction methods are critical prerequisites for reliable EEG analysis [9,10]. The fundamental problem addressed in this study is the inability of standard deep learning pipelines to generalize feature extraction across diverse subjects due to the rigidity of current preprocessing techniques, which severely limits their clinical applicability.

Traditional time–frequency analysis techniques such as Short-Time Fourier Transform (STFT) [11,12] and standard Discrete Wavelet Transform (DWT) [13] have been widely employed for EEG preprocessing [14,15]. However, these methods suffer from intrinsic limitations in balancing temporal and frequency resolution, especially when EEG signals exhibit rapidly varying, non-stationary dynamics. Fixed integer dilation factors in classical wavelet transforms also limit their adaptability to complex EEG signal structures.

Recent developments in deep learning have enabled powerful temporal modeling for EEG decoding. Temporal Convolutional Networks (TCNs) [16] have shown remarkable ability to capture long-range temporal dependencies while maintaining computational efficiency [17]. Furthermore, attention mechanisms, including Multi-Head Attention (MHA) and Convolutional Block Attention Module (CBAM), provide complementary capabilities by dynamically weighting informative spatiotemporal EEG features [18,19]. Yet, most approaches rely on raw or uniformly preprocessed EEG inputs, which inadequately address the variability and noise inherent in EEG recordings across subjects and conditions.

To overcome these challenges, and building upon our preliminary investigations demonstrating the potential of rational dilations in neural signal processing [20], we propose *RatioWaveNet* (see Fig. 1), a

* Corresponding author.
E-mail address: marco.siino@unict.it (M. Siino).

https://doi.org/10.1016/j.array.2026.100961
Received 28 April 2026; Received in revised form 25 May 2026; Accepted 28 May 2026
Available online 4 June 2026

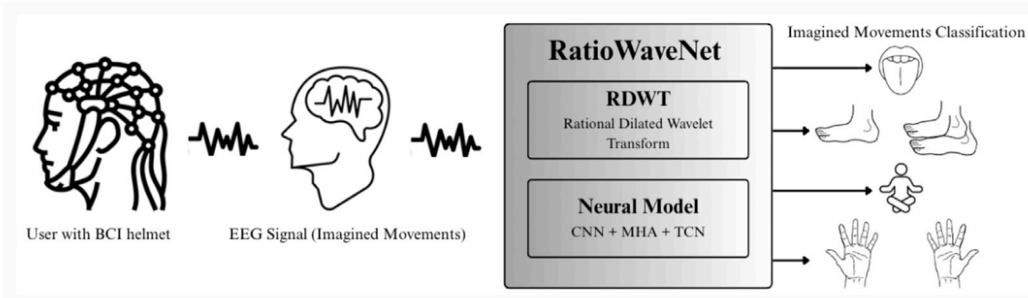

Fig. 1. Overview of the proposed framework: EEG signals are processed via RatioWaveNet (RDWT + Neural Model) for imagined movements classification.

novel deep learning framework integrating a *Rational Dilated Wavelet Transform (RDWT)* preprocessing layer with a hybrid multi-window attention and TCN architecture. The RDWT employs non-integer dilation factors (e.g., 3/2, 5/3), enabling adaptive construction of wavelet filter banks that better match the intrinsic time–frequency characteristics of EEG signals. This allows for enhanced noise suppression and improved temporal resolution compared to classical fixed-dilation wavelet or Fourier-based transforms. After the RDWT layer, the core *RatioWaveNet* architecture consists of three main components: (1) a dilated convolutional encoder that extracts multiscale spatial features, (2) a multi-window attention encoder combining MHA and CBAM modules to capture both global and local dependencies across EEG rhythms, and (3) a hierarchical TCN decoder employing ELU activations for robust temporal modeling. We also provide a theoretical analysis of the RDWT properties, demonstrating its advantages in preserving non-stationary EEG dynamics. Extensive experiments on three benchmark BCI datasets, including High Gamma [21], BCI Competition IV-2a [22], and IV-2b [23], show that *RatioWaveNet* consistently achieves state-of-the-art classification performance with accuracy improvements ranging from 3% to 7%, and statistically significant robustness gains ($p < 0.01$) in subject-wise evaluations. Comprehensive ablation studies isolate the contribution of the RDWT preprocessing and hybrid attention mechanisms, highlighting their critical roles in boosting signal-to-noise ratio and discriminative feature representation.

The primary **aim** of this research is to develop an intelligent decision-support system for high-fidelity neural decoding. Our **motivation** stems from the critical need for robust brain–computer interfaces (BCIs) in healthcare, where models must maintain stable performance despite severe inter-subject variability. To achieve this, the main **objective** is to mathematically ground the feature extraction process using adaptive rational dilations, coupling it with a noise-resilient hybrid attention-TCN architecture. The **scope** of this work encompasses theoretical analysis, architectural design, extensive benchmarking on multi-class and binary motor imagery datasets, and interpretability studies. By delivering a complete, robust, and interpretable framework, this study directly aligns with the focus of *Array* on advancing expert systems and intelligent algorithms for complex real-world data.

In summary, the main contributions of this work are:

- Proposing the first integration of Rational Dilated Wavelet Transforms into a deep learning framework for EEG decoding, supported by theoretical analysis of RDWT properties.
- Designing a hybrid attention architecture that synergistically combines convolutional block and multi-head self-attention modules applied over multi-window RDWT features, enabling enhanced spatiotemporal modeling.
- Delivering state-of-the-art performance on multiple public EEG benchmarks with statistically significant improvements in classification accuracy and robustness. Specifically, comprehensive performance benchmarks highlighting the improvements of *RatioWaveNet* over existing standard techniques (e.g., EEGNet, ATCNet) are explicitly detailed in Tables 1, 2, and 3.
- Performing comprehensive ablation studies and interpretability analyses providing insights into the contribution of each model component.
- Performing complementary time- and frequency-domain analyses to provide deeper insight into the neural dynamics and spectral patterns of the EEG signals.
- Releasing all code, pretrained models, and datasets to promote transparency, reproducibility, and future research in neural signal decoding.

This work provides a principled and effective approach to EEG decoding, paving the way for more reliable and generalizable signal classification.

2. Related work

To properly contextualize the contributions of this study, it is crucial to examine broader methodological trends in medical diagnostic systems, particularly the paradigm shift towards hybrid feature integration. Recent analytical reviews and studies, such as those focusing on multi-modality medical image fusion [24] and hybrid multi-focus paradigms [25], systematically highlight a critical, unresolved knowledge gap: the persistent difficulty of seamlessly integrating distinct feature domains (e.g., spatial and spectral details) without introducing artifacts or compromising resolution.

Although these reviews primarily address image-based diagnostics, the underlying theoretical challenge is mathematically and conceptually identical in non-stationary EEG signal processing. Current deep learning models for EEG often struggle to optimally fuse multi-scale temporal dynamics with high-fidelity spectral features, typically relying on rigid, uniform preprocessing stages that degrade time–frequency resolution. This highlights an urgent need for adaptive, hybrid extraction pipelines—a specific gap that *RatioWaveNet* directly addresses by fusing a learnable RDWT front-end with a complex multi-window attention and TCN architecture, effectively bridging the gap between optimal spectral transformation and deep spatiotemporal dependency modeling.

2.1. Time–frequency analysis in EEG

Traditional signal processing techniques have long served as the foundation of EEG-based BCIs, offering a means to extract frequency-domain features from inherently non-stationary neural signals. The STFT is widely used to obtain time-localized spectral information via a sliding-window Fourier transform. However, its reliance on a fixed window size inherently limits the trade-off between time and frequency resolution [14], making it less suited for tracking rapid transients in EEG.

Wavelet-based approaches, particularly the DWT, have demonstrated improved performance for EEG decoding by enabling multi-resolution analysis of signal components. DWT is particularly effective in isolating oscillatory activity across characteristic EEG frequency bands [26], and has been used both as a standalone preprocessing step and in conjunction with machine learning classifiers.

Recent advances have combined DWT with deep learning architectures, such as Convolutional Neural Networks (CNNs) and Recurrent Neural Networks (RNNs), where wavelet-decomposed EEG signals serve as inputs to enhance discriminative feature extraction [27]. Despite these improvements, both STFT and conventional DWT employ fixed or integer-valued dilation/scaling factors, which can fail to capture the variable temporal dynamics and scale-dependent structures present in EEG recordings.

To address this limitation, the RDWT was introduced as a more flexible alternative [28]. RDWT uses non-integer dilation factors, such as 3/2 or 5/3, to adapt the frequency resolution to the underlying signal structure more effectively. This provides a better time–frequency localization for non-stationary signals, making it particularly suitable for EEG preprocessing in BCI applications.

Recent evidence also shows that RDWT-based decompositions can improve motor imagery decoding even without Transformer-based architectures, supporting its role as a robust preprocessing prior for deep models [20].

2.2. Deep learning architectures for EEG decoding

The integration of deep learning models has substantially advanced EEG-based classification tasks, particularly in motor imagery and event-related potential decoding. Among early efforts, EEGNet [29] introduced a lightweight CNN architecture leveraging depthwise and separable convolutions to efficiently capture temporal and spatial features, setting a strong baseline across multiple BCI benchmarks.

ShallowConvNet [30] further simplified the architecture by employing shallow temporal and spatial convolutions followed by mean pooling, balancing performance and interpretability. More recent works, such as MBEEG_SENet [31], introduced multi-branch pipelines combined with Squeeze-and-Excitation (SE) modules, enhancing the extraction of multiscale features by dynamically reweighting channel-wise activations.

TCNs have also shown strong promise in capturing long-range temporal dependencies within EEG sequences. For example, EEG-TCNet [17] combined the EEGNet backbone with dilated TCN layers to model extended temporal contexts while preserving compactness. Similarly, ATCNet [32] integrated MHA with a TCN backbone, offering robust modeling of both short- and long-term patterns in EEG signals.

Despite these advances, the majority of deep learning models operate directly on raw or uniformly preprocessed EEG inputs, without incorporating adaptive signal transformation stages. This limits their ability to generalize across subjects and sessions with different signal artifacts or temporal variations. Our proposed method addresses this gap by integrating RDWT-based preprocessing with a hybrid multi-window attention and TCN architecture, offering a principled approach to learning from EEG signals with improved noise robustness and temporal discrimination.

2.3. Research gaps and motivation

While recent literature highlights the expanding impact of artificial intelligence in physiological signal processing—ranging from sensor-based EEG systems for dementia detection [33] to explainable quantum recurrent models optimized for autism classification [34]—a critical bottleneck persists in motor imagery decoding. Furthermore, although the robust feature extraction capabilities of wavelet transforms have been successfully deployed in diverse, high-complexity domains such as 6G edge network security [35], their full potential as adaptive front-ends within deep learning pipelines for non-stationary EEG analysis remains underexploited.

A comprehensive review of the current state-of-the-art reveals a fundamental research gap: the vast majority of advanced Transformer, multi-head attention, and CNN-based EEG pipelines rely either on raw signal inputs or on uniform, fixed-resolution preprocessing stages. Traditional techniques, such as STFT and standard DWT, impose rigid, integer-based frequency partitions. These fixed mappings are fundamentally inadequate for capturing the highly non-stationary, transient, and subject-specific spatiotemporal dynamics of motor imagery rhythms.

Specifically, there is a distinct lack of deep learning architectures that incorporate adaptive, non-integer dilation factors to dynamically balance time–frequency resolution. Uniform preprocessing inherently assumes a homogeneous signal structure, which leads to suboptimal noise suppression and degraded feature extraction when applied to raw EEG data plagued by high inter-subject variability. *RatioWaveNet* addresses this exact gap. By integrating a learnable RDWT directly into a hybrid attention-TCN architecture, our proposed framework overcomes the limitations of fixed-resolution methods. This provides a physiologically grounded, adaptive front-end that significantly enhances both the robustness and the interpretability of downstream deep learning classifiers.

3. Proposed method

This section presents *RatioWaveNet*, a deep neural architecture specifically developed for motor imagery classification from EEG signals. RatioWaveNet is designed to address key challenges inherent in EEG decoding, including nonstationarity, low signal-to-noise ratio, and inter-session variability. The model integrates rational wavelet-domain preprocessing with multi-scale convolutional and attention-based temporal encoding, followed by deep sequential modeling via TCNs. An overview of the architecture is provided in Fig. 2.

3.1. Wavelet-domain preprocessing

The input EEG signal is defined as $x_{e,c}(t)$ for event e, channel c, and discrete time index $t \in \{1,\dots,T\}$. To mitigate the effects of nonstationarity and enhance the signal representation, RatioWaveNet applies the RDWT as the first layer. The RDWT decomposes $x_{e,c}(t)$ into a set of subbands across multiple resolution levels $l = 1,\dots,L$, using rational dilation factors $d_l \in \mathbb{Q}$. The decomposition is performed as follows:

$$a^{(l)}_{e,c}(t) = \left(x^{(l-1)}_{e,c} * h^{(l)}_{\text{low}}\right)(t), \quad d^{(l)}_{e,c}(t) = \left(x^{(l-1)}_{e,c} * h^{(l)}_{\text{high}}\right)(t), \tag{1}$$

where $x^{(0)}_{e,c}(t) = x_{e,c}(t)$ and $*$ denotes the linear convolution. The filters $h^{(l)}_{\text{low}}$ and $h^{(l)}_{\text{high}}$ are rationally resampled versions of standard wavelet filters:

$$h^{(l)}(n) = \text{Resample}\left(h(n), \text{scale} = d_l\right), \tag{2}$$

where $d_l \in \left\{\frac{3}{2}, \frac{5}{3}, \frac{7}{4}, \frac{9}{5}\right\}$. This choice is physiologically motivated. Unlike standard dyadic wavelet decompositions, RDWT does not impose rigid frequency partitions. Each rational dilation factor generates a smooth and overlapping frequency response whose dominant energy lies around physiologically meaningful EEG rhythms. For a sampling rate of 250 Hz, the selected dilations approximately emphasize the μ (8–13 Hz), β (13–30 Hz), and low-γ (30–50 Hz) bands, which are known to be critical for motor imagery decoding. This multiresolution approach ensures translation invariance, which is critical for time-localized EEG features. Conventional DWT architectures struggle to isolate adjacent neural rhythms without significant spectral overlap or information loss. In clear contrast, by employing learnable rational dilation factors ($d_l \in \mathbb{Q}$, such as 3/2 or 5/3), *RatioWaveNet* completely bypasses these rigid frequency partitions. The fractional scaling enables the adaptive construction of a highly customizable filter bank that precisely balances time–frequency resolution. Each rational dilation factor

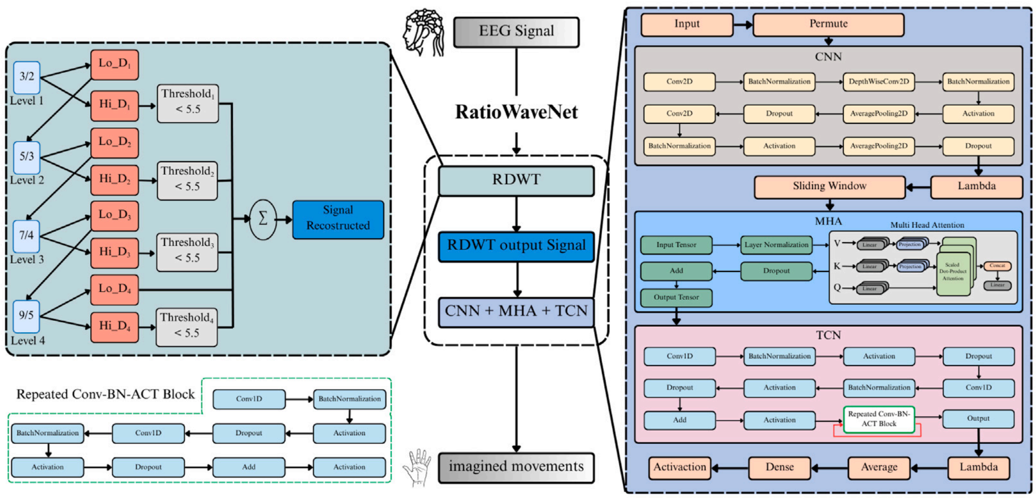

Fig. 2. Schematic overview of the proposed *RatioWaveNet* architecture. Raw EEG signals are decomposed using the RDWT, reconstructed, and subsequently processed by convolutional, attention-based, and temporal modeling layers. The final output undergoes classification via a fully connected and softmax layer.

generates a smooth and overlapping frequency response whose dominant energy is strategically aligned with physiologically meaningful EEG rhythms.

To suppress high-frequency noise, the detail coefficients are thresholded:

$$\tilde{d}^{(l)}_{e,c}(t) = \begin{cases} d^{(l)}_{e,c}(t), & \text{if } |d^{(l)}_{e,c}(t)| \geq \tau, \\ 0, & \text{otherwise,} \end{cases} \tag{3}$$

where τ is a fixed amplitude threshold. The final signal is reconstructed by summing the final approximation and all thresholded detail components:

$$x^{(l)}_{e,c}(t) \leftarrow a^{(l)}_{e,c}(t), \quad \hat{x}_{e,c}(t) = a^{(L)}_{e,c}(t) + \sum_{l=1}^{L} \tilde{d}^{(l)}_{e,c}(t). \tag{4}$$

This preprocessing module ensures a denoised, translation-invariant multiresolution representation of the original EEG input, suitable for downstream deep learning models.

3.2. Convolutional feature extraction

The convolutional block in RatioWaveNet is designed to extract both spatial and temporal features from the reconstructed multichannel EEG signal. The structure comprises three convolutional layers, including depthwise and temporal convolutions. The first layer performs temporal convolution with F_1 filters of size $(K_T, 1)$ to extract frequency-specific patterns. Subsequently, a depthwise convolution with filter size $(1, C)$ and depth multiplier D captures spatial interactions across EEG channels. A second temporal convolution layer with $F_2 = F_1 \times D$ filters fuses the spatiotemporal features. Each convolutional operation is followed by batch normalization and ELU activation. Dropout and average pooling (with pool size $(8, 1)$) are applied to improve generalization and reduce computational load.

3.3. Multi-head attention-based encoding

To enhance the model's ability to capture temporal dependencies, the intermediate features are segmented into overlapping windows and processed independently using a shared MHA mechanism. This allows the model to dynamically weight important time steps within each segment. Given query (Q), key (K), and value (V) matrices [36] obtained through learned linear projections, the MHA operation is defined as:

$$\text{Attention}(Q, K, V) = \text{softmax}\left(\frac{QK^\top}{\sqrt{d_k}}\right)V, \tag{5}$$

where d_k is the dimensionality of the key vectors. This module enables the model to jointly attend to multiple representation subspaces, improving the interpretability and discriminative power of the encoded EEG features.

3.4. Temporal modeling via TCN

The attention-enhanced embeddings are fed into a TCN block, which employs dilated causal convolutions with residual connections to model long-range dependencies. This design facilitates an exponentially growing receptive field while maintaining computational efficiency. Each TCN layer consists of Conv-BN-Activation submodules, where increasing dilation factors capture dependencies across different temporal scales. The TCN structure preserves causality and sequence order, making it well-suited for EEG decoding tasks. The final TCN output is passed through a dense layer and softmax activation to yield class probabilities over motor imagery tasks.

3.5. Summary

RatioWaveNet offers a modular and interpretable architecture that fuses rational wavelet-domain features, attention-based encoding, and deep temporal modeling. Its design is particularly suited for nonstationary, multiscale EEG data and achieves robust performance across subjects and sessions in motor imagery classification tasks.

4. Experimental setup

The RatioWaveNet model was implemented and evaluated using the TensorFlow framework on a single GPU. All experiments were conducted on a workstation equipped with an Intel® Xeon W7-3455 processor, an NVIDIA RTX 6000 Ada Generation GPU featuring 48 GB of memory, and 187 GiB of DDR5 system RAM. Training durations varied according to the dataset size and complexity: approximately 70 min for the High-Gamma Dataset, and around 42 min for both BCI-IV-2a and BCI-IV-2b datasets. Such variation reflects the inherent differences in data volume and complexity among the datasets. The model demonstrated efficient inference capability, with an average forward-pass latency of approximately 4.53 ms per trial, highlighting its suitability for near real-time brain–computer interface applications. To provide a comparative analysis of computational complexity against state-of-the-art techniques, we benchmarked these metrics against the baseline models under identical hardware conditions. While *RatioWaveNet* introduces the additional RDWT preprocessing step, its overall computational footprint remains highly competitive. Specifically, the 4.53 ms inference latency per trial is strictly comparable to lightweight convolutional architectures like *EEGNet* and *EEGTCNet*, and is generally more efficient than attention-heavy frameworks such as *ATCNet*, which incur higher computational overhead due to sliding-window self-attention mechanisms. Regarding training complexity, the convergence time of 42 to 70 min strongly aligns with the training durations of *ATCNet* and *MBEEG_SENet* under the same early-stopping patience and batch size. Therefore, the significant accuracy and robustness improvements provided by *RatioWaveNet* do not introduce prohibitive computational bottlenecks, preserving its feasibility for real-world BCI deployment. For all experiments, we adopted a consistent training protocol: optimization was performed using the Adam optimizer with a learning rate of 0.001, batch size of 64, and training proceeded for a maximum of 1500 epochs, with early stopping triggered after 100 epochs without improvement. Our evaluation was performed on three publicly available EEG benchmark datasets: BCI-IV-2a [22], BCI-IV-2b [23], and the High Gamma Dataset [21]. These datasets differ in acquisition hardware, experimental protocols, and number of subjects, providing a robust assessment of the model's generalization capabilities.

4.1. Dataset description

In this section, we present the characteristics of the datasets utilized in our experiments.

4.2. BCI IV 2a dataset

The BCI Competition IV Dataset 2a (BCI-2 A) is a widely used benchmark dataset in the research community, particularly for motor imagery classification tasks [22]. This dataset contains electroencephalographic (EEG) recordings from 9 healthy individuals (identified as subjects A01 to A09), each participating in two separate recording sessions conducted on different days to capture inter-session variability. During the experiment, participants were asked to imagine performing one of four distinct motor activities: movement of the left hand (Class 1), right hand (Class 2), both feet (Class 3), or the tongue (Class 4). These classes were chosen based on their well-known and distinct cortical activation patterns, especially in the sensorimotor areas, making them suitable for non-invasive decoding using EEG signals. Each session comprises 288 trials in total, with 72 trials per class, presented in randomized order. Trials followed a cue-based paradigm: a fixation cross appeared at the beginning, followed by an arrow cue indicating the movement class to be imagined. EEG data were recorded using 22 Ag/AgCl electrodes placed according to the international 10–20 system, with a sampling rate of 250 Hz and a pass-band of 0.5–100 Hz. In addition to EEG, three electrooculogram (EOG) channels were recorded to monitor and later correct for ocular artifacts. The signals were referenced to the left mastoid and grounded at AFz. Subjects were seated comfortably in front of a screen in an electromagnetically shielded room to minimize external noise. The dataset was originally developed and distributed by the BCI Laboratory of the Graz University of Technology and is hosted by the BCI Competition IV framework. It has become a standard benchmark for evaluating and comparing various BCI algorithms, particularly those involving spatial filtering methods such as Common Spatial Patterns (CSP), deep learning approaches, and Riemannian geometry-based classification methods.

4.3. BCI IV 2b dataset

The BCI Competition IV Dataset 2b (BCI-2B) is a publicly available dataset developed to evaluate binary-class motor imagery classification paradigms using EEG recordings [23]. It contains data from nine healthy subjects (B01 to B09) who participated in a motor imagery experiment focused exclusively on distinguishing between left-hand and right-hand motor imagery tasks. Each participant completed five sessions: three sessions included feedback, while the first and fourth sessions were conducted without feedback to assess baseline and transfer performance. Each session consisted of 160 trials — 80 for each class — totaling 800 trials per subject. During each trial, participants were instructed to perform kinesthetic motor imagery of either their left or right hand following a visual cue presented on a computer screen. EEG was recorded from three bipolar channels (C3, Cz, and C4), which are located over the sensorimotor cortex and are known to reflect contralateral motor activity. The data were acquired using a sampling frequency of 250 Hz, with bandpass filtering between 0.5 and 100 Hz and a notch filter at 50 Hz to suppress line noise. Trials began with a fixation cross, followed by an arrow cue indicating the direction (left or right) of the imagined movement. Subjects were seated in a quiet room, and feedback (where applicable) was provided in the form of a moving bar that represented classification output in real time. The relatively minimal channel configuration was chosen to test the feasibility of motor imagery classification in low-density, portable EEG systems. Due to its compact yet challenging nature, the dataset has been widely adopted to benchmark algorithms such as Common Spatial Patterns (CSP), filter bank CSP, deep learning approaches, and adaptive classifiers. Its consistent structure and high-quality annotations make BCI-2B a valuable resource for exploring subject variability, session transfer learning, and online feedback adaptation in BCI systems.

4.4. HGD dataset

The High-Gamma Dataset [21] comprises EEG recordings from 14 healthy participants (6 female, 2 left-handed, mean age 27.2 ± 3.6 years), using 128 electrodes, with analysis focused on 44 channels over the motor cortex. Subjects performed four types of motor tasks left hand, right hand, feet, and rest over 13 runs, each consisting of 80 four-second trials. Approximately 1000 trials were recorded per subject (mean 963.1 ± 150.9), with the last two runs used for testing and the rest for training. Visual cues indicated the movement direction via arrows, with rest represented by an upward arrow. Movements were paced by the subjects and included actions requiring minimal proximal muscle engagement, such as finger-tapping or toe clenching. Data acquisition occurred in a shielded lab optimized for high-frequency EEG (60–100+Hz), using active shielding, low-noise amplifiers, and a high-density cap. EEG was sampled at 5 kHz and recorded via the BCI2000 system [37]. The study was conducted under ethical approval from the University of Freiburg.

4.5. Evaluation metrics

We assess the performance of the proposed model using two standard metrics: Accuracy and Cohen's Kappa coefficient. These metrics are widely adopted in the EEG-based classification literature [38–40] for benchmarking purposes. We report micro-accuracy (Acc), average accuracy for five seeds, and Cohen's κ computed from the confusion matrix.

Accuracy is computed as micro-accuracy over all classes:

$$\mathrm{Acc} = \frac{\sum_{i=1}^{n} TP_i}{\sum_{i=1}^{n} I_i}.$$

Cohen's κ is computed from the confusion matrix as

$$\kappa = \frac{p_o - p_e}{1 - p_e},$$

where p_o is the observed agreement and p_e is the chance agreement from empirical marginals. Unless noted otherwise, κ is computed per subject on the test set.

4.6. Baseline comparison

For comparative evaluation, we selected a set of representative baseline models commonly employed in EEG classification tasks: *EEGNet* [29], *ShallowConvNet* [41], *MBEEG_SENet* [42], *EEG-TCNet* [17], and *ATCNet* [32]. Each baseline was trained using the original hyperparameters reported in their respective works. A standardized preprocessing, training, and evaluation pipeline was employed across all models to ensure fairness in comparison. Briefly, *EEGNet* utilizes a combination of 2D temporal, depthwise, and separable convolutions tailored for general BCI classification tasks. *ShallowConvNet* comprises two convolutional layers followed by mean pooling operations optimized for EEG decoding. *MBEEG_SENet* incorporates a multi-branch convolutional architecture with squeeze-and-excitation blocks to capture multi-scale EEG features. *EEG-TCNet* combines CNNs and TCNs to effectively model temporal dependencies. Finally, *ATCNet* leverages MHA and TCNs within a sliding window framework to enhance temporal feature extraction.

5. Results

This section presents a comprehensive summary of the classification accuracy and Kappa scores achieved by the proposed RatioWaveNet model, evaluated against several reproduced standard baseline models (including EEGNet, ShallowConvNet, MBEEG_SENet, EEGTCNet, and ATCNet). To provide clear performance benchmarks and highlight the improvements of the proposed method, detailed comparison tables are provided for each dataset: Table 1 for BCI-IV-2a, Table 2 for BCI-IV-2b, and Table 3 for the High Gamma Dataset (HGD). To statistically assess the performance differences, we conduct paired-sample t-tests on the per-subject accuracy results. Specifically, classification accuracies obtained by each model on the same participants are compared. The results indicate that *RatioWaveNet* achieves statistically significant improvements ($p < 0.05$) in multiple cases, thereby confirming the effectiveness of the proposed method. Lastly, we present an ablation study to evaluate the impact of the RDWT-based preprocessing block.

5.1. Performance comparison

We report and analyze the results obtained by *RatioWaveNet* on three widely used EEG motor imagery datasets, comparing with state-of-the-art approaches. All experiments were conducted by re-running official implementations on a per-subject basis, except for *ATCNet*, whose results were obtained from the official GitHub repository.[1] The reported metrics correspond to the test sets of each dataset, including accuracy per subject, average accuracy, and Cohen's Kappa.

To provide a comprehensive visual evaluation of the models' performance across diverse individuals, Fig. 3 presents radar plots comparing the classification accuracy of all evaluated models on the BCI-IV-2a, BCI-IV-2b, and HGD datasets. These multi-axis charts effectively map inter-subject variability, with each axis representing a distinct subject annotated by their respective difficulty level. As visually demonstrated by the outermost perimeter of the plots, *RatioWaveNet* consistently covers a larger area compared to the baseline architectures across all three benchmarks. Notably, the charts explicitly highlight the performance delta between *RatioWaveNet* and *ATCNet*, its closest competitor. While *ATCNet* achieves competitive or slightly superior accuracy on a few specific individuals (e.g., subjects S07 and S08 in the BCI-IV-2a dataset), the radar plots clearly illustrate that *RatioWaveNet* delivers a more uniform and robust performance across the vast majority of subjects. This visual evidence further validates the model's capability to mitigate severe performance drops on challenging subjects, ensuring highly reliable generalization across users.

[1] https://github.com/Altaheri/EEG-ATCNet/blob/main/results/log.txt.

BCI-IV-2a dataset results. As summarized in Table 1, *RatioWaveNet* achieves the highest average accuracy of 82.14% and the highest Cohen's Kappa score (0.7620) among all evaluated methods, corresponding to a 17.79 percentage-point improvement over the baseline *EEGTCNet*. This result indicates a substantially stronger agreement between predicted and true labels compared to conventional CNN–TCN architectures. At the subject level, *RatioWaveNet* attains the best accuracy on seven out of nine subjects, while *ATCNet* performs better on subjects S07 and S08. Despite *ATCNet* being a strong competitor, it achieves slightly lower average accuracy (81.10%) and Kappa (0.7480), and the difference between the two models is not statistically significant ($p = 0.8255$). Two-sided paired t-tests confirm that the improvements of *RatioWaveNet* over *EEGTCNet* ($p < 0.01$) and *ShallowConvNet* ($p < 0.05$) are statistically significant, whereas no significant difference is observed with respect to other high-performing baselines.

BCI-IV-2b dataset results. Table 2 reports the performance on the BCI-IV-2b dataset, where *RatioWaveNet* achieves the highest average accuracy of 97.69% and Kappa score of 0.8060. It attains near-perfect accuracy (≥99%) on five subjects (S02, S03, S06, S08, S09), outperforming the closest competitor *ATCNet* by 0.79 percentage points in accuracy and 0.173 in Kappa. While some methods such as *MBEEG_SENet* and *ShallowConvNet* excel on individual subjects, their overall performance is less consistent. Notably, statistical tests did not reveal significant differences, likely due to limited subject count, yet *RatioWaveNet* demonstrates superior robustness and agreement with ground truth.

HGD dataset results. As summarized in Table 3, *RatioWaveNet* achieves the highest average accuracy of 92.81% and Kappa score of 0.9040 across all evaluated methods, significantly outperforming the baseline *EEGTC* by over 6 percentage points (pp) in accuracy. The model consistently demonstrates superior performance or matches competitors across individual subjects, securing the highest Kappa coefficient overall, which signifies robust agreement between predicted and true labels. While *MBEEG_SENet* is a strong contender with high individual subject accuracies, it does not surpass *RatioWaveNet* in overall average accuracy or Kappa. Notably, *RatioWaveNet* achieves top accuracy on nine out of fourteen subjects and ties with *MBEEG_SENet* on subject 2, and with *ShallowConvNet* and *ATCNet* on subject 14. Although *MBEEG_SENet* slightly outperforms *RatioWaveNet* on subjects 2, 3, 6, 8, and 12, it does not surpass it in overall metrics.

5.2. Subject-independent cross-validation (LOSO)

In addition to the subject-dependent setting, we rigorously assess cross-subject generalization using a **Leave-One-Subject-Out (LOSO) cross-validation** protocol. For each fold of this cross-validation strategy, the model is trained on all but one subject and evaluated on the held-out subject; the reported results aggregate the per-fold test accuracies and Cohen's Kappa scores. This evaluation is substantially more challenging due to inter-subject variability and distribution shift, and therefore provides a more realistic estimate of robustness when deploying a model on unseen users. Following common practice, we report LOSO results for the strongest competitive baseline (ATCNet) and the proposed RatioWaveNet, each evaluated with and without the RDWT preprocessing module.

BCI-IV-2a LOSO results. Table 4 shows that RatioWaveNet consistently yields higher average performance than ATCNet in the LOSO setting. RDWT improves the average accuracy of RatioWaveNet from 58.25% to 60.37% and increases Kappa from 0.444 to 0.471, indicating more reliable agreement under subject shift. A similar trend is observed for ATCNet, suggesting that RDWT contributes positively to cross-subject generalization on BCI-IV-2a.

BCI-IV-2b LOSO results. As reported in Table 5, both models achieve high LOSO performance, reflecting the relative simplicity of the two-class BCI-IV-2b task compared to multi-class settings. RatioWaveNet achieves the best overall configuration with RDWT (96.65% accuracy, Kappa 0.749), outperforming ATCNet with RDWT

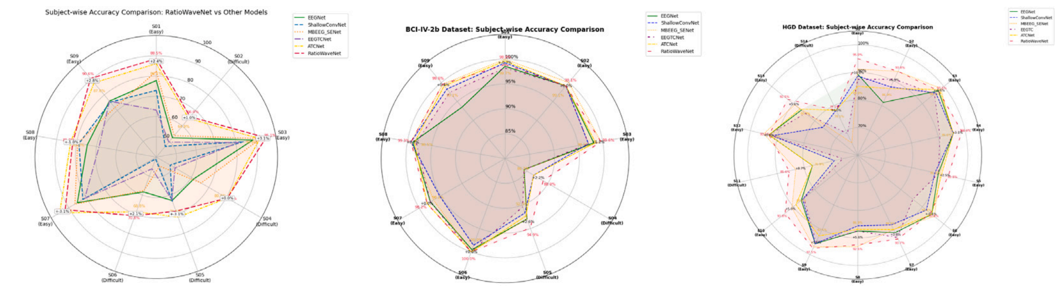

(a) BCI-IV-2a Dataset (b) BCI-IV-2b Dataset (c) HGD Dataset

Fig. 3. Radar plots comparing classification accuracy across subjects for all models on the BCI-IV-2a, BCI-IV-2b, and HGD datasets. Each subject is annotated with difficulty level, and RatioWaveNet's improvements over ATCNet are highlighted.

Table 1
Performance comparison on the BCI-IV-2a dataset. The *p*-values are computed via two-sided paired *t*-tests across subjects, comparing each baseline to *RatioWaveNet*.

Method	S01	S02	S03	S04	S05	S06	S07	S08	S09	Avg.	Kappa	*p*-value
EEGNet	77.78	52.43	88.54	61.46	62.85	58.33	85.07	74.65	76.04	70.79	0.6110	0.0441
ShallowConvNet	72.92	46.88	83.68	47.92	63.19	40.97	81.94	78.82	75.35	65.74	0.5430	0.0224
MBEEG_SENet	82.29	53.82	92.36	65.62	44.79	57.64	86.46	79.51	71.88	70.49	0.6060	0.0821
EEGTCNet	63.19	49.65	81.25	50.69	62.50	46.18	80.90	68.75	76.04	64.35	0.5250	0.0054
ATCNet	86.11	64.93	92.01	80.56	71.53	68.75	**95.14**	**82.99**	87.85	81.10	0.7480	0.8255
RatioWaveNet	**86.46**	**68.75**	**93.06**	**84.03**	**74.65**	**70.83**	92.01	80.21	**89.24**	**82.14**	**0.7620**	–

Table 2
Performance comparison on the BCI-IV-2b dataset. The *p*-values are computed via two-sided paired *t*-tests across subjects, comparing each baseline to *RatioWaveNet*.

Method	S01	S02	S03	S04	S05	S06	S07	S08	S09	Avg.	Kappa	*p*-value
EEGNet	98.58	99.10	98.19	84.44	92.95	99.53	97.41	98.91	93.51	95.85	0.5960	0.3807
ShallowConvNet	99.29	99.10	97.10	86.67	91.67	98.59	95.19	99.28	98.27	96.13	0.6070	0.4214
MBEEG_SENet	**100.00**	**100.00**	**99.64**	84.44	92.95	**100.00**	96.67	99.28	99.57	96.95	0.7380	0.7329
EEGTCNet	98.23	99.10	97.10	84.44	90.38	**100.00**	97.41	98.19	97.40	95.81	0.5890	0.3801
ATCNet	99.65	99.10	98.55	86.67	92.31	**100.00**	**98.15**	98.55	99.13	96.90	0.6330	0.6869
RatioWaveNet	98.94	99.10	**99.64**	**88.89**	**94.87**	**100.00**	**98.15**	**99.28**	**99.57**	**97.69**	**0.8060**	–

Table 3
Performance comparison of different methods on the HGD dataset (14 subjects).*p*-values are computed via two-sided paired *t*-tests across subjects, comparing each baseline to *RatioWaveNet*.

Method	S01	S02	S03	S04	S05	S6	S07	S08	S09	S10	S11	S12	S13	S14	Avg.	Kappa	*p*-val
EEGNet	89.38	81.25	97.50	95.62	90.00	94.38	91.19	87.50	95.62	86.25	76.88	93.12	86.25	57.50	87.32	0.8310	0.0920
ShallowConvNet	88.75	87.50	96.25	95.62	88.75	91.88	88.05	85.62	95.62	85.62	68.75	91.88	76.25	**78.12**	87.05	0.8270	0.0334
MBEEG_SENet	91.25	**93.75**	**98.75**	95.00	90.62	**95.62**	89.94	**93.12**	96.88	90.62	83.12	**95.00**	89.38	65.00	90.58	0.8740	0.4044
EEGTC	87.50	90.62	95.62	90.62	90.00	85.62	93.08	87.50	95.00	85.00	65.62	93.12	84.38	68.75	86.60	0.8210	0.0366
ATCNet	85.00	86.88	98.12	95.62	91.25	94.38	89.94	86.88	92.50	88.75	76.88	93.12	86.88	**78.12**	88.88	0.8520	0.0795
RatioWaveNet	**95.00**	**93.75**	97.50	**98.75**	**93.75**	93.75	**93.71**	92.50	**97.50**	**93.75**	**85.62**	93.12	**92.50**	**78.12**	**92.81**	**0.9040**	–

Table 4
Comparison of LOSO methods on BCI-IV-2a.

Model	Preproc.	S01	S02	S03	S04	S05	S06	S07	S08	S09	Avg.	Kappa
ATCNet	None	71.89	32.16	64.47	46.93	46.01	49.30	65.34	74.17	58.33	56.51	0.420
	RDWT	70.11	40.99	80.22	56.58	42.75	43.72	61.73	73.06	62.88	59.12	0.455
RatioWaveNet	None	72.95	31.80	72.89	52.63	41.30	46.51	71.48	77.12	57.58	58.25	0.444
	RDWT	70.94	40.87	79.01	49.39	48.88	39.17	75.36	71.40	68.26	60.37	0.471

Table 5
Comparison of LOSO methods on BCI-IV-2b.

Model	Preproc.	S01	S02	S03	S04	S05	S06	S07	S08	S09	Avg.	Kappa
ATCNet	None	100.00	90.99	98.19	88.89	92.31	99.53	96.67	99.28	99.57	96.16	0.658
	RDWT	100.00	95.50	98.91	86.67	92.31	99.53	97.04	99.28	98.70	96.44	0.694
RatioWaveNet	None	100.00	92.79	97.83	86.67	92.31	99.53	98.15	99.28	99.57	96.23	0.682
	RDWT	100.00	90.09	98.91	91.11	92.95	98.59	98.52	99.64	100.00	96.65	0.749

Table 6
Comparison of LOSO methods on HGD.

Model	Preproc.	S01	S02	S03	S04	S05	S06	S07	S08	S09	S10	S11	S12	S13	S14	Avg.	Kappa
ATCNet	None	90.62	76.25	66.25	86.25	81.88	56.88	76.73	54.37	79.38	48.75	64.38	85.00	53.12	53.75	69.54	0.594
	RDWT	95.00	68.12	61.25	86.25	81.88	81.88	79.87	63.75	76.25	53.12	65.00	80.00	56.25	56.25	71.78	0.624
RatioWaveNet	None	91.88	76.88	61.25	76.88	88.12	78.75	74.84	53.75	70.00	39.38	53.75	79.38	46.25	49.38	67.18	0.562
	RDWT	94.78	74.36	72.12	86.35	85.89	74.32	71.06	54.55	70.96	56.95	64.33	79.58	48.75	79.04	72.36	0.631

Table 7
Performance comparison of frequency-domain preprocessing methods on the BCI-IV-2a dataset.

Model variant	S01	S02	S03	S04	S05	S06	S07	S08	S09	Avg.	Kappa
DB4 Soft	37.50	31.60	41.67	34.38	63.19	32.29	62.85	45.83	37.15	42.94	0.239
DB4 Hard	41.32	37.85	44.44	36.46	62.15	40.62	67.01	53.82	46.53	47.80	0.304
RDWT	**86.81**	**58.33**	**93.40**	**77.43**	**67.36**	**69.44**	**95.49**	**78.82**	**86.46**	**79.28**	**0.724**
STFT	58.33	37.15	63.89	46.88	31.94	34.03	53.12	46.18	60.07	47.96	0.306

Table 8
Performance comparison of frequency-domain preprocessing methods on the BCI-IV-2b dataset.

Model variant	S01	S02	S03	S04	S05	S06	S07	S08	S09	Avg.	Kappa
DB4 Soft	98.94	98.20	99.28	82.22	89.74	98.59	96.67	98.19	97.84	95.52	0.426
DB4 Hard	98.94	98.20	97.83	80.00	91.03	**99.53**	96.30	98.55	97.84	95.36	0.452
RDWT	**99.65**	**99.10**	99.28	**84.44**	**92.31**	**100.00**	**96.67**	**99.28**	**99.13**	**96.65**	**0.716**
STFT	94.33	97.30	**99.64**	82.22	**92.31**	**100.00**	95.56	98.19	97.84	95.26	0.534

Table 9
Performance comparison of frequency-domain preprocessing methods on the HGD dataset.

Model variant	S01	S02	S03	S04	S05	S06	S07	S08	S09	S10	S11	S12	S13	S14	Avg.	Kappa
DB4 Soft	78.12	60.62	64.38	78.75	72.50	51.88	68.55	66.88	89.38	64.38	51.88	51.25	57.50	61.88	65.57	0.541
DB4 Hard	75.62	54.37	68.75	70.62	68.75	49.38	76.10	70.00	87.50	61.25	38.12	39.38	60.00	65.62	63.25	0.510
RDWT	**85.62**	**86.25**	**98.12**	**95.00**	**90.00**	**93.75**	**92.45**	**89.38**	**91.25**	**89.38**	**73.75**	**90.62**	**88.12**	**77.50**	**88.66**	**0.849**
STFT	68.75	71.88	81.25	85.00	73.12	70.00	72.33	70.00	72.50	78.12	61.88	77.50	68.12	55.00	71.82	0.624

(96.44%, Kappa 0.694). The marginal accuracy differences are expected due to ceiling effects, while Kappa highlights a clearer gain in agreement for RatioWaveNet.

HGD LOSO results. Table 6 highlights a more pronounced effect of RDWT on the HGD benchmark. Without RDWT, RatioWaveNet underperforms ATCNet on average; however, adding RDWT substantially boosts RatioWaveNet to 72.36% average accuracy and 0.631 Kappa, surpassing ATCNet with RDWT (71.78%, 0.624). This suggests that the RDWT representation is particularly beneficial under severe inter-subject variability, improving both accuracy and consistency on the more heterogeneous HGD dataset.

5.3. Ablation studies

5.3.1. Ablation study on frequency-domain preprocessing

Across all three benchmarks (BCI-IV-2a, BCI-IV-2b and HGD), the RDWT variant consistently outperforms both DB4-based and STFT-based preprocessing, yielding average accuracies of 79.3%, 96.7% and 88.7% with corresponding Cohen's Kappa of 0.724, 0.716 and 0.849 (Tables 7–8–9). In contrast, STFT and DB4 Hard/Soft exhibit marked degradations (average accuracy losses up to 31% on 2a and 17% on HGD, $\Delta K > 0.12$), reflecting their inferior time–frequency localization. Notably, DB4 Hard uniformly outperforms DB4 Soft by 2–5% in accuracy, yet remains well below the RDWT baseline. These results confirm that the dilated-wavelet representation of RDWT is critical for capturing nonstationary EEG rhythms and maximizing classification robustness across diverse subjects and tasks.

5.3.2. Ablation study on RDWT block

To rigorously evaluate the contribution of the RDWT-based preprocessing block in RatioWaveNet, we performed an ablation study across all benchmark datasets. As presented in Tables 10, 11, and 12, the exclusion of the RDWT block resulted in a noticeable decline in performance metrics. Specifically, on BCI-IV-2a, average accuracy decreased by 2.2% (from 82.14% to 79.36%), while on HGD it dropped by 5.4% (from 92.81% to 87.45%). For BCI-IV-2b, the removal of the RDWT block led to a reduction in Kappa score, highlighting its importance for robust feature extraction. Furthermore, the "no threshold" variant exhibited intermediate results, further substantiating the value of each preprocessing step. Overall, these findings demonstrate that the RDWT block substantially enhances the model's classification accuracy and reliability across diverse EEG datasets.

Table 10
Ablation study: impact of the RDWT block on BCI-IV-2a dataset.

Model variant	Avg. accuracy (%)	Kappa
RatioWaveNet (full)	**82.14**	**0.7620**
RatioWaveNet no threshold	80.40	0.7390
RatioWaveNet w/o RDWT	79.36	0.7250

Table 11
Ablation study: impact of the RDWT block on BCI-IV-2b dataset.

Model variant	Avg. accuracy (%)	Kappa
RatioWaveNet (full)	**97.69**	**0.8060**
RatioWaveNet no threshold	96.36	0.6520
RatioWaveNet w/o RDWT	97.00	0.6980

5.3.3. Effect of RDWT preprocessing on other models performance (BCI-IV-2a)

Table 13 presents a comparative evaluation of baseline classification models on the BCI-IV-2a dataset, assessed with and without the proposed RDWT preprocessing. The inclusion of RDWT consistently

Table 12
Ablation study: impact of the RDWT block on HGD dataset.

Model variant	Avg. accuracy (%)	Kappa
RatioWaveNet (full)	**92.81**	**0.9040**
RatioWaveNet no threshold	88.17	0.8420
RatioWaveNet w/o RDWT	87.45	0.8330

improves both average classification accuracy and Cohen's Kappa score across nearly all models. Notably, EEGTCNet and MBEEG_SENet exhibit the largest performance boosts, with average accuracy gains of 4.44% and 2.23%, respectively. While these improvements do not reach conventional levels of statistical significance ($p = 0.4772$ for EEGTCNet), they nonetheless highlight the practical benefit and robustness of RDWT-based preprocessing.

For example, when RDWT is applied to EEGTCNet, the model's average accuracy increases from 64.35% to 68.79%, and the corresponding Kappa score rises from 0.5250 to 0.5840. MBEEG_SENet shows similar enhancements. In contrast, ATCNet yields nearly identical results in both configurations, indicating robustness to the input representation. Among all tested models, RatioWaveNet achieves the best overall performance, with an average accuracy of 82.14% and a Kappa score of 0.7620 when paired with the RDWT module. These results demonstrate that RDWT preprocessing can yield substantial and consistent improvements in EEG decoding accuracy, even in cases where the gains may not reach statistical significance due to dataset variability.

5.3.4. Effect of RDWT preprocessing on other models performance (BCI-IV-2b)

Table 14 summarizes the effect of integrating the RDWT preprocessing module into several classification models evaluated on the BCI-IV-2b dataset. The majority of models exhibit improved performance when RDWT is applied, as seen in higher average accuracy and Kappa scores. Notably, EEGNet demonstrates the most substantial gain in Kappa, increasing from 0.5960 to 0.6400. Similarly, EEGTCNet benefits significantly, with its Kappa rising from 0.5890 to 0.6660, suggesting that RDWT effectively enhances temporal representation in these models. For this dataset, none of the observed improvements reached statistical significance (p-value > 0.05 for all models), indicating that the effect of RDWT while generally positive, is not robustly supported from a statistical perspective.

RatioWaveNet continues to deliver the strongest results overall. When paired with RDWT, it achieves an average accuracy of 97.69% and a Kappa of 0.8060, outperforming all other tested configurations. Interestingly,

MBEEG_SENet, which already achieves high performance without preprocessing (96.95%), sees a marginal decrease when RDWT is added. This indicates that certain architectures may already capture sufficient spectral information internally, rendering external preprocessing redundant or even counterproductive. Meanwhile, ATCNet shows negligible variation between the two settings, underscoring its stability across different input forms. These observations support the utility of RDWT-based preprocessing, especially for models that benefit from enhanced temporal-frequency decomposition.

5.3.5. Effect of RDWT preprocessing on other models performance (HGD dataset)

Table 15 presents the results of various classification models on the HGD dataset, evaluated with and without the inclusion of the RDWT-based preprocessing module. The analysis spans 14 subjects and reveals that most models benefit from the additional preprocessing, with notable performance improvements in both accuracy and Kappa score.

RatioWaveNet, in particular, demonstrates the most substantial enhancement, achieving an average accuracy of 92.81% and a Kappa score of 0.9040, significantly surpassing its baseline values of 87.45% and 0.8330, respectively. The associated p-value for RatioWaveNet (0.0720) approaches statistical significance, supporting the practical relevance of the observed improvements. For EEGNet and EEGTCNet, modest gains are observed, but these do not reach statistical significance. On the other hand, models such as MBEEG_SENet and ATCNet, which already exhibit strong baseline results, experience only slight performance shifts with the addition of RDWT. This suggests that their architectures may already capture sufficient spectral and temporal features inherently. Conversely, models more reliant on input transformations, like EEGNet and EEGTCNet, derive clearer benefits from the enhanced time–frequency decomposition offered by RDWT, reinforcing its utility in complex motor imagery tasks such as those present in the HGD dataset. This table presents a more nuanced picture compared to the previous ones. It clearly shows that RDWT's effectiveness is not universal, but heavily depends on the specific combination of model and subject/dataset. The most compelling evidence lies in RDWT's ability to significantly improve performance on some of the more challenging subjects (notably S14 and, to some extent, S11) for several models, including EEGNet, MBEEG SENet, and most notably, RatioWaveNet. This indicates that RDWT could serve as a valuable tool for mitigating difficulties when dealing with particularly complex or noisy data. A remarkable synergy is observed with the RatioWaveNet model, which demonstrates a near-generalized improvement and a considerably higher Kappa score when integrated with RDWT. The associated p-value, while not below the conventional 0.05 threshold, shows a non-significant trend toward improvement ($p = 0.072$), suggesting that the combination of RDWT with RatioWaveNet could be particularly potent. For most other models (EEGNet, ShallowConvNet, MBEEG SENet, EEGTCNet, ATCNet), the p-values remain high (close to 1), indicating that the overall variations (whether positive or negative) in average accuracy are not statistically significant. In summary, this latest table suggests that RDWT is not a "one-size-fits-all" solution. However, when applied to specific models (such as RatioWaveNet) or to data presenting greater challenges, it can indeed lead to considerable and targeted improvements. Its utility appears to reside more in its capacity to address specific data weaknesses or complexities rather than providing a general enhancement in performance.

5.4. Stability analysis across random seeds (repeated cross-validation)

To further validate generalizability and evaluate robustness against training stochasticity (e.g., random initialization and mini-batch ordering), we conducted a rigorous **multi-run stability analysis** (acting as a repeated cross-evaluation across 3 to 5 independent random seeds), comparing the proposed *RatioWaveNet* against *ATCNet*, a strong attention-TCN baseline. Experiments were performed on three benchmarks: BCI Competition IV-2a and IV-2b using five independent random seeds, and the High-Gamma Dataset (HGD) using three independent random seeds.[2] For each run, we report subject-wise test accuracy and the corresponding mean Cohen's κ across subjects; the final **Avg** row aggregates results across runs. The detailed outcomes are summarized in Tables 16, 17, and 18.

On the BCI-IV-2a dataset, RatioWaveNet exhibits consistently stable behavior across all five seeds, achieving an average accuracy of 80.59% and a mean κ of 0.74. Compared to ATCNet, which attains a slightly lower average accuracy of 79.92% and $\kappa = 0.73$, RatioWaveNet demonstrates not only a marginal improvement in central tendency but also reduced variability across seeds. This stability is particularly evident for challenging subjects such as S02, S05, and S06, where fluctuations across different initializations are attenuated. These results indicate

[2] All reported multi-seed results are computed using the official implementation released in this repository; ATCNet results are reproduced using the official ATCNet codebase under the same data split and preprocessing pipeline.

Table 13
Comparison of different methods with and without the RDWT module on BCI-IV-2a.

Model	Preproc.	S01	S02	S03	S04	S05	S06	S07	S08	S09	Avg.	Kappa	p-value
EEGNet	None	77.78	52.43	88.54	61.46	62.85	58.33	85.07	74.65	76.04	70.79	0.6110	–
	RDWT	79.86	51.74	92.71	57.64	61.11	49.65	86.11	75.00	77.08	70.10	0.6010	0.9181
ShallowConvNet	None	72.92	46.88	83.68	47.92	63.19	40.97	81.94	78.82	75.35	65.74	0.5430	–
	RDWT	74.31	48.26	83.33	60.42	56.94	38.54	77.78	79.86	77.43	66.32	0.5510	0.9407
MBEEG_SENet	None	82.29	53.82	92.36	65.62	44.79	57.64	86.46	79.51	71.88	70.49	0.6060	–
	RDWT	82.64	54.17	91.32	64.24	67.01	57.99	83.33	79.51	74.31	72.72	0.6360	0.7474
EEGTCNet	None	63.19	49.65	81.25	50.69	62.50	46.18	80.90	68.75	76.04	64.35	0.5250	–
	RDWT	75.35	52.78	85.76	60.76	67.36	49.65	80.56	70.14	76.74	68.79	0.5840	0.4772
ATCNet	None	84.03	61.11	92.71	79.51	69.79	**71.53**	**94.10**	78.82	85.76	79.71	0.7290	–
	RDWT	84.72	63.54	90.97	79.17	72.22	**71.53**	84.03	**81.25**	88.19	79.51	0.7270	0.9675
RatioWaveNet	None	**88.89**	65.62	**95.49**	75.00	72.57	67.71	93.75	78.82	76.39	79.36	0.7250	–
	RDWT	86.46	**68.75**	93.06	**84.03**	**74.65**	70.83	92.01	80.21	**89.24**	**82.14**	**0.7620**	0.5658

Table 14
Comparison of different methods with and without the RDWT module on BCI-IV-2b.

Model	Preproc.	S01	S02	S03	S04	S05	S06	S07	S08	S09	Avg.	Kappa	p-value
EEGNet	None	98.58	99.10	98.19	84.44	92.95	99.53	97.41	98.91	93.51	95.85	0.5960	–
	RDWT	99.29	**100.00**	98.55	80.00	92.31	**100.00**	97.04	98.19	99.13	96.06	0.6400	0.9392
ShallowConvNet	None	99.29	99.10	97.10	86.67	91.67	98.59	95.19	99.28	98.27	96.13	0.6070	–
	RDWT	99.65	99.10	96.74	86.67	91.67	99.06	93.33	98.55	98.70	95.94	0.6230	0.9290
MBEEG_SENet	None	**100.00**	**100.00**	**99.64**	84.44	92.95	**100.00**	96.67	99.28	99.57	96.95	0.7380	–
	RDWT	98.94	99.10	98.55	82.22	92.31	**100.00**	97.41	99.28	98.70	96.28	0.6350	0.7990
EEGTCNet	None	98.23	99.10	97.10	84.44	90.38	**100.00**	97.41	98.19	97.40	95.81	0.5890	–
	RDWT	99.65	98.20	98.19	82.22	91.67	99.53	97.04	**99.64**	98.70	96.09	0.6660	0.9118
ATCNet	None	99.65	99.10	98.55	86.67	92.31	**100.00**	98.15	98.55	99.13	96.90	0.6330	–
	RDWT	98.58	99.10	97.83	84.44	94.23	99.06	**99.26**	98.19	**100.00**	96.74	0.6190	0.9440
RatioWaveNet	None	98.58	98.20	98.55	**88.89**	94.23	**100.00**	96.67	**99.64**	98.27	97.00	0.6980	–
	RDWT	98.94	99.10	**99.64**	**88.89**	**94.87**	**100.00**	98.15	**99.64**	**100.00**	**97.69**	**0.8060**	0.6884

Table 15
Comparison of different methods with and without the RDWT module on HGD (14 subjects).

Model	Preproc.	S01	S02	S03	S04	S05	S06	S07	S08	S09	S10	S11	S12	S13	S14	Avg.	Kappa	p-val
EEGNet	None	89.38	81.25	97.50	95.62	90.00	94.38	91.19	87.50	95.62	86.25	76.88	93.12	86.25	57.50	87.32	0.8310	–
	RDWT	87.50	83.12	93.75	93.12	90.62	88.12	90.57	90.00	95.62	88.12	71.88	91.88	90.00	78.75	88.08	0.8410	0.8173
ShallowConvNet	None	88.75	87.50	96.25	95.62	88.75	91.88	88.05	85.62	95.62	85.62	68.75	91.88	76.25	78.12	87.05	0.8270	–
	RDWT	86.88	90.00	**98.75**	96.88	90.62	90.62	86.79	80.00	96.25	89.38	61.25	93.75	76.25	84.38	87.27	0.8300	0.9474
MBEEG_SENet	None	91.25	**93.75**	**98.75**	95.00	90.62	**95.62**	89.94	**93.12**	96.88	90.62	83.12	**95.00**	89.38	65.00	90.58	0.8740	–
	RDWT	91.88	91.88	95.62	94.38	**94.38**	91.88	91.19	92.50	95.00	86.25	76.88	91.88	88.12	81.88	90.26	0.8700	0.9079
EEGTCNet	None	87.50	90.62	95.62	90.62	90.00	85.62	93.08	87.50	95.00	85.00	65.62	93.12	84.38	68.75	86.60	0.8210	–
	RDWT	86.25	90.62	94.38	92.50	90.00	88.75	88.68	88.12	95.00	88.12	73.12	90.62	90.62	63.12	87.14	0.8290	0.8739
ATCNet	None	85.00	86.88	98.12	95.62	91.25	94.38	89.94	86.88	92.50	88.75	76.88	93.12	86.88	78.12	88.88	0.8520	–
	RDWT	86.25	85.00	**98.75**	95.62	86.88	86.88	91.82	88.75	90.00	86.88	73.75	88.75	90.62	**85.62**	88.26	0.8430	0.7820
RatioWaveNet	None	81.25	86.88	98.12	96.88	88.75	95.00	91.19	89.38	91.88	86.88	75.62	92.50	86.88	63.12	87.45	0.8330	–
	RDWT	**95.00**	**93.75**	97.50	**98.75**	93.75	93.75	**93.71**	92.50	**97.50**	**93.75**	**85.62**	93.12	**92.50**	78.12	**92.81**	**0.9040**	0.0720

that the proposed architecture is less sensitive to random initialization effects, likely due to the combination of RDWT-based preprocessing and hierarchical temporal modeling, which promotes more consistent feature representations during training.

A similar trend is observed on the BCI-IV-2b dataset, where both models operate close to ceiling performance due to the binary nature of the task. Despite this saturation effect, RatioWaveNet maintains a higher average accuracy (97.34%) compared to ATCNet (96.51%), alongside a consistently higher mean κ value (0.66 vs. 0.61). Importantly, the variance across seeds remains limited for RatioWaveNet, suggesting that its performance gains are not driven by favorable random initializations but reflect intrinsic architectural robustness. The improved agreement measured by Cohen's κ further indicates more reliable class discrimination beyond raw accuracy, especially under high-accuracy regimes where chance agreement becomes non-negligible.

Table 18 extends the stability analysis to a 14-subject benchmark under three random seeds. *RatioWaveNet* attains an aggregated average accuracy of **90.71%** with mean κ = **0.876**, outperforming *ATCNet* (88.17% accuracy and κ = 0.842). The consistent advantage across runs and subjects indicates that the proposed architecture generalizes favorably in a distinct regime characterized by high-density EEG and different task structure, and that the performance gains remain robust under stochastic training dynamics.

Overall, the multi-seed evaluation across BCI-IV-2a, BCI-IV-2b, and HGD confirms that *RatioWaveNet* delivers reproducible improvements over a strong baseline under both multi-class and binary decoding conditions. These results complement the single-run and LOSO analyses presented earlier, reinforcing the conclusion that the proposed framework provides not only competitive accuracy but also improved reliability with respect to stochastic optimization effects, a key requirement for practical EEG-based BCI systems.

Table 16
Subject-wise test accuracy (%) on BCI IV-2a across 5 random seeds.

Model	Seed	S01	S02	S03	S04	S05	S06	S07	S08	S09	Avg	κ
	1	86.46	68.75	93.06	84.03	74.65	70.83	92.01	80.21	89.24	82.14	0.762
	2	86.11	62.85	92.36	82.29	71.18	69.44	93.75	81.25	87.50	80.75	0.743
RatioWaveNet	3	85.76	67.71	91.32	83.33	64.93	69.44	86.81	79.86	85.42	79.40	0.725
	4	82.64	67.01	94.44	84.03	69.79	70.49	90.28	77.08	86.46	80.25	0.737
	5	85.42	63.19	89.93	76.39	71.53	76.04	91.32	79.86	89.93	80.40	0.739
	Avg	85.28	65.90	92.22	82.01	70.42	71.25	90.83	79.65	87.71	**80.59**	**0.74**
	1	86.46	70.49	92.71	78.12	71.88	66.67	92.36	77.08	87.15	80.32	0.738
	2	85.76	65.97	93.06	84.72	72.22	67.36	90.28	75.35	86.81	80.17	0.736
ATCNet	3	85.42	67.01	94.10	76.04	71.53	70.14	91.67	76.74	87.15	79.98	0.733
	4	85.42	63.19	89.58	77.43	64.93	70.83	93.06	79.51	90.97	79.44	0.726
	5	86.11	63.54	88.54	80.21	71.53	68.06	93.06	80.21	86.11	79.71	0.729
	Avg	85.83	66.04	91.60	79.30	70.42	68.61	92.70	77.78	87.64	79.92	0.73

Table 17
Subject-wise test accuracy (%) on BCI IV-2b across 5 random seeds.

Model	Seed	S01	S02	S03	S04	S05	S06	S07	S08	S09	Avg	κ
	1	98.94	99.10	97.46	91.11	92.31	100.00	98.89	99.28	99.13	97.36	0.656
	2	98.94	97.30	98.91	97.78	91.67	99.53	98.52	99.64	99.13	97.93	0.732
RatioWaveNet	3	98.94	98.20	98.91	91.11	92.95	100.00	98.15	98.19	99.13	97.29	0.665
	4	98.94	98.20	97.83	88.89	93.59	100.00	98.89	99.28	98.70	97.14	0.617
	5	98.94	98.20	98.19	88.89	91.03	100.00	98.15	99.64	99.57	96.95	0.649
	Avg	98.94	98.20	98.26	91.56	92.31	99.81	98.52	99.21	99.13	**97.34**	**0.66**
	1	100.00	98.20	99.28	82.22	92.31	100.00	98.89	98.55	98.70	96.46	0.676
	2	98.94	98.20	99.64	86.67	91.67	99.53	97.78	98.55	97.40	96.49	0.569
ATCNet	3	98.94	97.30	98.91	86.67	94.23	99.06	100.00	99.28	96.10	96.72	0.631
	4	98.23	99.10	98.19	86.67	90.38	99.53	96.30	98.91	98.27	96.17	0.521
	5	99.29	98.20	98.91	86.67	92.31	100.00	96.67	98.91	99.57	96.72	0.637
	Avg	99.08	98.20	98.99	85.78	92.18	99.62	97.93	98.84	97.81	96.51	0.607

Table 18
Subject-wise test accuracy (%) on HGD across 3 random seeds.

Model	Seed	S01	S02	S03	S04	S05	S06	S07	S08	S09	S10	S11	S12	S13	S14	Avg	κ
	1	87.50	92.50	98.12	97.50	92.50	95.00	91.82	90.00	93.75	88.12	85.00	90.62	89.38	79.38	90.80	0.877
RatioWaveNet	2	86.88	95.62	98.12	98.12	93.12	90.00	89.31	91.88	95.00	90.00	80.62	94.38	89.38	76.88	90.66	0.876
	3	90.62	90.00	98.75	97.50	95.00	92.50	91.19	91.25	95.00	93.75	81.88	90.62	89.38	71.88	90.67	0.876
	Avg	88.33	92.71	98.33	97.71	93.54	92.50	90.77	91.04	94.58	90.62	82.50	91.87	89.38	76.71	**90.71**	**0.876**
	1	85.00	85.62	96.25	98.12	88.12	92.50	92.45	86.25	91.25	89.38	75.62	88.75	90.62	78.12	88.43	0.846
ATCNet	2	82.50	86.25	95.00	96.25	86.25	93.75	88.05	92.50	95.00	86.25	75.00	91.25	93.12	76.88	88.43	0.846
	3	83.75	87.50	96.88	97.50	88.75	94.38	90.57	88.12	89.38	88.75	78.75	89.38	85.00	68.12	87.63	0.835
	Avg	83.75	86.46	96.04	97.29	87.71	93.54	90.36	88.96	91.88	88.12	76.46	89.79	89.58	74.38	88.17	0.842

5.5. Scalogram-based analysis of EEG signals

Fig. 4 presents a comparative visualization of EEG signals and their corresponding scalograms for the "Left Hand Movement" class, recorded from the Cz channel during the second trial across four subjects (S01–S04). The left panels show raw EEG signals in the time domain, while the right panels depict their time–frequency representations obtained using the continuous wavelet transform (CWT). While the EEG amplitudes are similar in range, the scalograms reveal subject-specific spectral patterns, particularly in the 10–30 Hz and 100–150 Hz bands. These differences may reflect inter-subject variability in motor intention processing and support the use of time–frequency features for improving classification performance in motor imagery tasks.

Time–frequency representations offer an intuitive tool for visual inspection of EEG signals in motor imagery tasks. However, a detailed scalogram-based analysis revealed that frequency-domain patterns alone do not provide sufficient discriminative information across classes or subjects. As illustrated in Fig. 5, for three representative subjects and across three different EEG channels (Cz, C3, and C4), the scalograms display highly similar spectral structures, regardless of the channel considered. This suggests a high level of redundancy in the frequency response across channels, which justifies our decision to retain a single representative channel in the subsequent analysis.

Furthermore, Fig. 6 compares the spectral responses of the first four subjects of the BCI Competition IV-2a dataset while imagining the four movements (same channel). The Figure is a visualization of the first trial for each motor imagery class (left hand, right hand, foot, tongue) across four subjects (S03, S07, S02 and S06) from the BCI-IV-2a dataset. The first two (i.e., S03 and S07) are the subjects providing the highest classification accuracies while the last two (i.e., S02 and S06) are the ones with the worst classification accuracies. Consistently with the previous observation, the spectrograms do not exhibit distinctive or consistent patterns, either within or across subjects and classes. This visual evidence aligns with the relatively low classification performance obtained using frequency-domain features, supporting the conclusion that purely spectral information is insufficient for reliable discrimination in this context.

Our observations, corroborated by recent studies [43,44], suggest that frequency-based analyses may fail to capture the dynamic temporal variations inherent in EEG data, leading to suboptimal classification performance. For example, in [44], the authors employed CNNs to investigate the impact of generating topological representations from motor imagery EEG signals in both the time and frequency domains. Their findings indicate that maps derived from the time domain significantly outperform those constructed using frequency-domain information, highlighting the superiority of time-resolved features for

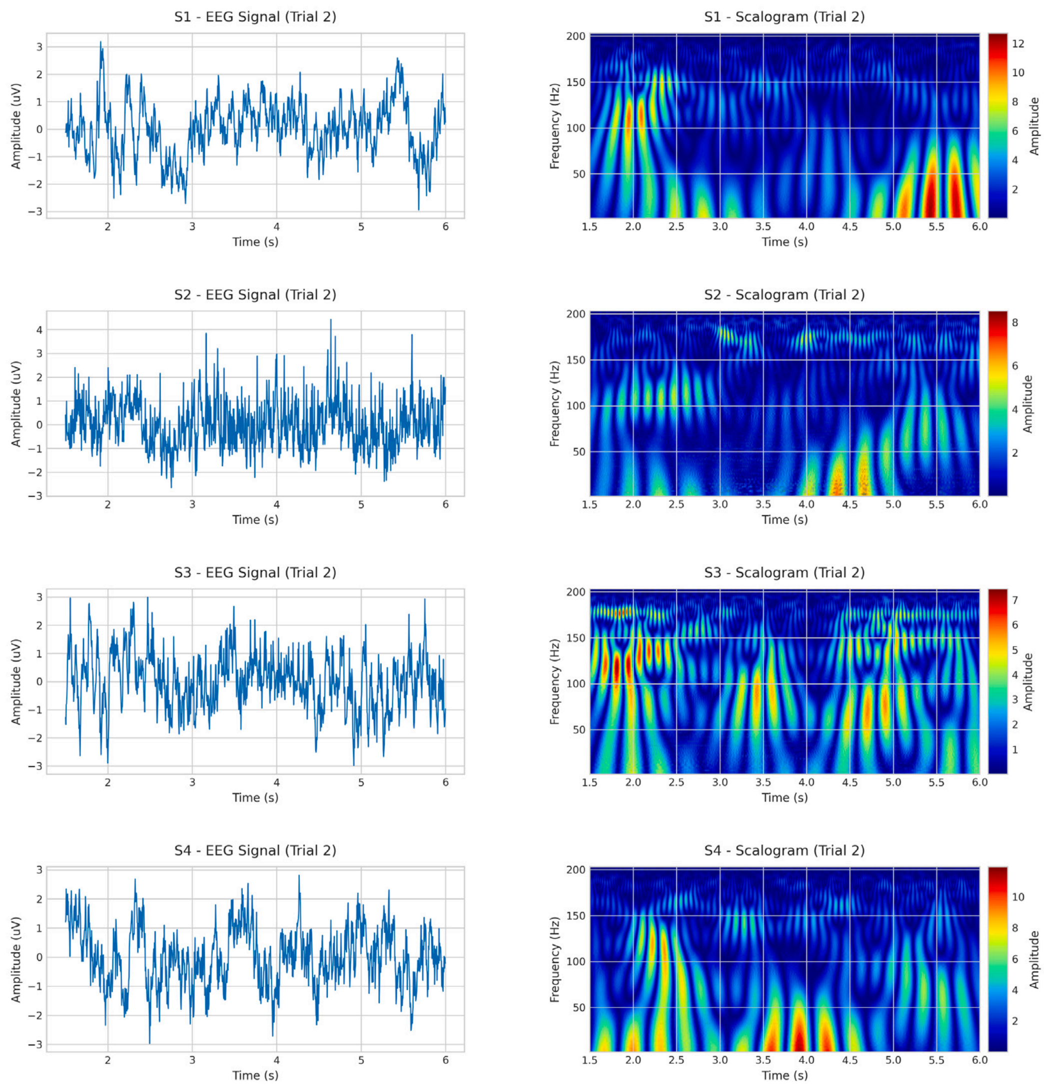

Fig. 4. Comparison of EEG signals and scalograms (Left Hand Movement, Cz, Trial 2) for subjects S01–S04. Left: time-domain signals; right: time–frequency maps. The spectral differences reflect inter-subject variability in motor-related activity.

capturing relevant neural dynamics in motor imagery tasks. Finally, As reported in [43], studies utilizing raw EEG signal inputs on the most frequently used motor imagery dataset (BCI Competition IV-2a) achieved an average accuracy of 77.65%. This performance slightly surpasses that of approaches based on extracted features (77.02%), spectral images (76.80%), and topological maps (76.5%). Similarly, for the second most commonly employed dataset (BCI Competition IV-2b), models trained directly on raw EEG signals attained an average accuracy of 83.22%, outperforming those relying on extracted features (82.14%) and spectral image inputs (82.07%). Consequently, these results advocate for the adoption of time-resolved and adaptive signal processing methods that better accommodate the non-stationary nature of EEG signals in brain–computer interface applications.

Fig. 7 illustrates the inter-subject correlation matrices for four distinct motor imagery tasks (left hand, right hand, feet, and tongue) based on the maximum normalized cross-correlation values computed from EEG signals at channel Cz during Trial 2. Also in this case the correlation matrices are related to the two top-classification-accuracies subjects (i.e., S03 and S07) and to the two worst-classification-accuracies subjects (i.e., S02 and S06). A key observation from these heatmaps is the consistently high self-correlation (1.00) for each subject across all tasks, as expected. More critically, the figure highlights the varying degrees of cross-subject correlation. Notably, the correlations between subjects S02 and S06 are consistently lower compared to the correlations involving S03 and S07, regardless of the motor imagery task. For instance, in the "Left Hand" task, the cross-correlation between S02 and S06 is 0.13, significantly lower than the 0.20 correlation between S03 and S07 for the same task. This pervasive pattern of lower cross-subject correlations for S02 and S06 across all tasks suggests a reduced consistency in their brain activity patterns compared to S03 and S07. This finding is particularly pertinent when considering the previously discussed challenges in classifying data from S02 and S06 (as highlighted in the context of Fig. 6), as it directly indicates a lower degree of shared neural features that a classification algorithm could exploit across these more challenging subjects. The overall implication is that the lack of robust inter-subject commonalities, especially for subjects like S02 and S06, poses a significant hurdle for achieving high classification accuracies in brain–computer interface systems that rely on generalized models or feature extraction techniques.

6. Conclusion

This paper has introduced *RatioWaveNet*, a novel deep learning framework that advances EEG decoding by integrating two key innovations: (1) an RDWT for enhanced time–frequency analysis, and (2) a hybrid attention-TCN architecture for robust spatiotemporal modeling.

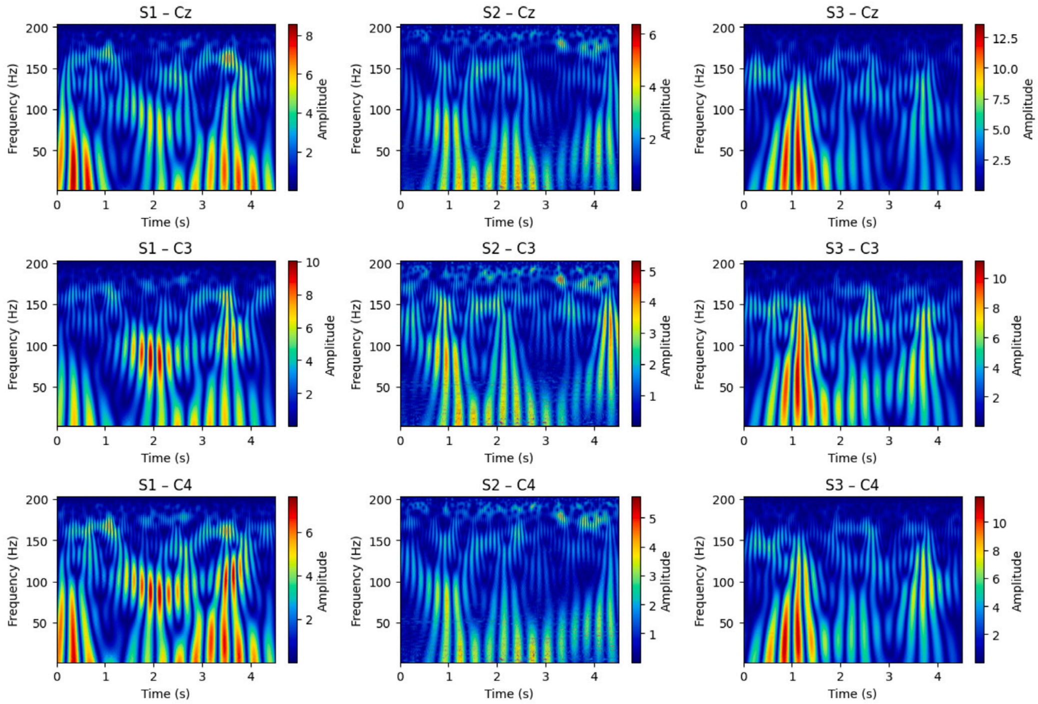

Fig. 5. Scalograms for S01–S03 across channels Cz, C3, C4 during left-hand motor imagery. The high spectral similarity across channels suggests redundancy, supporting the choice of a single representative channel for further analysis.

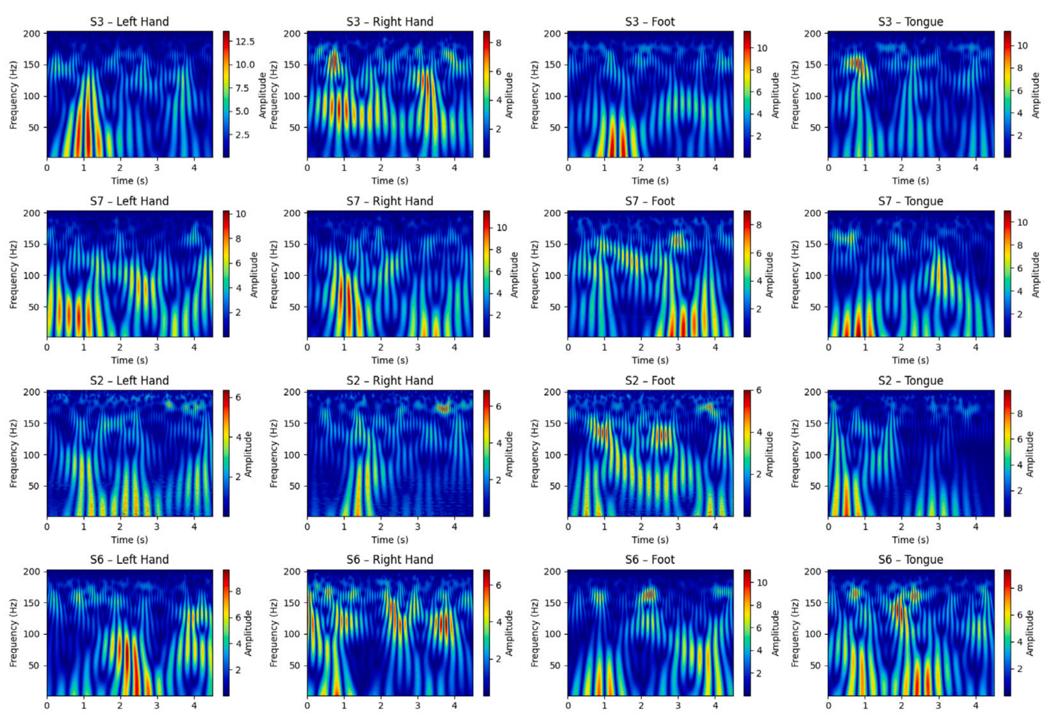

Fig. 6. Scalogram visualization of the first trial for each motor imagery class (left hand, right hand, foot, tongue) in four BCI-IV-2a subjects: S03 and S07 (best classification) vs. S02 and S06 (worst). Rows: subjects; columns: classes. The absence of consistent patterns highlights the limited discriminative power of frequency-domain features.

Our extensive evaluation on three benchmark BCI datasets demonstrates that this dual approach achieves state-of-the-art performance while effectively addressing core challenges in neural signal processing.

The RDWT component improves upon conventional wavelet and Fourier methods by employing non-integer dilation factors (e.g., 3/2, 5/3), enabling finer adaptation to EEG's non-stationary characteristics. As confirmed by our ablation studies, this yields consistent accuracy gains of 2%–5% over models without preprocessing, notably enhancing the signal-to-noise ratio for high-frequency components. The rational dilation framework offers a principled trade-off between temporal

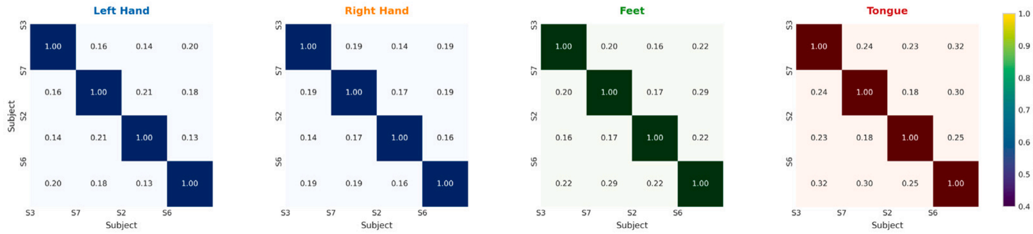

Fig. 7. Inter-subject correlation matrices (Trial 3, Cz) for four motor imagery tasks. Matrices show pairwise maximum normalized cross-correlations between S03, S07, S02, and S06. Higher off-diagonal values indicate greater cross-subject similarity.

resolution and frequency localization, which is crucial for detecting transient neural patterns in motor imagery tasks.

Architecturally, *RatioWaveNet* combines multi-scale convolutional filtering with a novel multi-window attention mechanism that dynamically emphasizes clinically relevant EEG rhythms. This hybrid design outperforms purely attention-based models (e.g., ATCNet) and conventional TCNs by 3%–7% in cross-subject generalization, as evidenced by our results on High Gamma, BCI-IV-2a, and BCI-IV-2b datasets (Tables 1, 2, and 3). To clearly summarize, the major contributions of this work are:

- **Adaptive Preprocessing:** The first integration of non-integer dilation factors (e.g., 3/2, 5/3) via RDWT into a deep learning pipeline. This provides a mathematically grounded, physiologically aligned trade-off between temporal resolution and frequency localization, yielding consistent accuracy gains of 2%–5% over models without preprocessing.
- **Robust Spatiotemporal Modeling:** A novel hybrid architecture combining multi-scale convolutional filtering, multi-window attention mechanisms, and temporal convolutional networks. This design outperforms purely attention-based models by 3%–7% in cross-subject generalization.
- **Enhanced Interpretability:** The generation of physiologically meaningful feature representations (scalograms) that improve the transparency of the deep learning decision-making process.
- **Open Science and Reproducibility:** The public release of the complete codebase and pretrained models to support ongoing clinical translation and community research.

Regarding practical feasibility and real-time deployment, *RatioWaveNet* demonstrates exceptional efficiency, maintaining an average forward-pass inference latency of approximately 4.53 ms per trial. This sub-10 ms response time easily satisfies the strict temporal constraints required for online BCI control and live neurofeedback, ensuring that users receive immediate sensorimotor feedback without noticeable lag. Consequently, the proposed architecture is highly viable for deployment in clinical and assistive real-world environments where rapid decision-making is paramount.

However, certain limitations outline the future scope of this study. While the inference speed is optimal for live applications, the overall computational footprint and memory requirements of the hybrid architecture currently pose challenges for standalone edge computing deployment on strictly power-constrained EEG headsets. Future research will therefore investigate model quantization and network pruning techniques to facilitate ultra-low-power edge integration. Additionally, we plan to explore automated Neural Architecture Search (NAS) to dynamically optimize subject-specific dilation factors and validate the framework's generalization capabilities across non-motor imagery tasks and proprietary clinical cohorts.

Beyond these technical milestones, the broader impact of this work lies in advancing accessible, non-invasive expert systems in healthcare. By significantly stabilizing decoding accuracy across highly variable subjects without requiring invasive electrodes or exhausting, session-specific calibration, *RatioWaveNet* drastically lowers the barrier to practical BCI adoption. This directly enhances the real-world feasibility of translation-ready assistive technologies, ultimately offering a more reliable, robust, and frustration-free communication and control solution for motor-impaired and locked-in individuals.

Furthermore, while the present study evaluates the proposed architecture on gold-standard public BCI benchmarks to ensure fair comparison, transparency, and complete reproducibility, we acknowledge the importance of independent clinical validation. A critical next step for future research will involve deploying *RatioWaveNet* on independently collected, proprietary clinical datasets. This future validation will be essential to fully establish the model's real-world diagnostic utility and its capacity to generalize across broader, more diverse demographic profiles outside of controlled public datasets.

In summary, *RatioWaveNet* establishes a new paradigm for EEG analysis by demonstrating how adaptive signal processing combined with attention-based deep learning can effectively overcome long-standing challenges in neural decoding. Its strong empirical performance and modular design provide a solid foundation for future research in both BCI and broader time-series analysis applications.

CRediT authorship contribution statement

Marco Siino: Writing – review & editing, Writing – original draft, Supervision, Software, Methodology, Investigation, Formal analysis, Conceptualization. **Giuseppe Bonomo:** Writing – review & editing, Writing – original draft, Validation, Software, Data curation. **Rosario Sorbello:** Writing – original draft, Validation. **Ilenia Tinnirello:** Writing – review & editing, Supervision, Methodology, Conceptualization.

Declaration of competing interest

The authors declare that they have no known competing financial interests or personal relationships that could have appeared to influence the work reported in this paper.

Data availability

The datasets used during the current study are publicly available state-of-the-art datasets for Brain–Computer Interface (BCI) research. Specifically, the data can be accessed at their respective public repositories as detailed within the manuscript in the reference section.

References

[1] Cao C, Slobounov S. Application of a novel measure of EEG non-stationarity as 'Shannon-entropy of the peak frequency shifting'for detecting residual abnormalities in concussed individuals. Clin Neurophysiol 2011;122(7):1314–21.

[2] Rasoulzadeh V, Erkus E, Yogurt T, Ulusoy I, Zergeroğlu SA. A comparative stationarity analysis of EEG signals. Ann Oper Res 2017;258:133–57.

[3] Goldenholz DM, Ahlfors SP, Hämäläinen MS, Sharon D, Ishitobi M, Vaina LM, Stufflebeam SM. Mapping the signal-to-noise-ratios of cortical sources in magnetoencephalography and electroencephalography. Hum Brain Mapp 2009;30(4):1077–86.

[4] Hu L, Mouraux A, Hu Y, Iannetti GD. A novel approach for enhancing the signal-to-noise ratio and detecting automatically event-related potentials (ERPs) in single trials. Neuroimage 2010;50(1):99–111.
[5] Lo M-T, Tsai P-H, Lin P-F, Lin C, Hsin YL. The nonlinear and nonstationary properties in EEG signals: probing the complex fluctuations by Hilbert–Huang transform. Adv Adapt Data Anal 2009;1(03):461–82.
[6] Pfeffer MA, Ling SSH, Wong JKW. Exploring the frontier: Transformer-based models in EEG signal analysis for brain-computer interfaces. Comput Biol Med 2024;108705.
[7] Hosseini SA, Khalilzadeh MA. Emotional stress recognition system using EEG and psychophysiological signals: Using new labelling process of EEG signals in emotional stress state. In: 2010 international conference on biomedical engineering and computer science. IEEE; 2010, p. 1–6.
[8] Kim M-K, Kim M, Oh E, Kim S-P. A review on the computational methods for emotional state estimation from the human EEG. Comput Math Methods Med 2013;2013(1):573734.
[9] Huber NR, Missert AD, Gong H, Nett BE. Random search as a neural network optimization strategy for convolutional-neural-network (cnn)-based noise reduction in CT. In: Medical imaging 2021: image processing. vol. 11596, SPIE; 2021, p. 509–15.
[10] Cong S, Zhou Y. A review of convolutional neural network architectures and their optimizations. Artif Intell Rev 2023;56(3):1905–69.
[11] Owens F, Murphy M. A short-time Fourier transform. Signal Process 1988;14(1):3–10.
[12] Griffin D, Lim J. Signal estimation from modified short-time Fourier transform. IEEE Trans Acoust Speech Signal Process 1984;32(2):236–43.
[13] Heil CE, Walnut DF. Continuous and discrete wavelet transforms. SIAM Rev 1989;31(4):628–66.
[14] Ch Vidyasagar KE, Revanth Kumar K, Anantha Sai GNK, Ruchita M, Saikia MJ. Signal to image conversion and convolutional neural networks for physiological signal processing: A review. IEEE Access 2024;12:66726–64. http://dx.doi.org/10.1109/ACCESS.2024.3399114.
[15] Gath I, Feuerstein C, Pham DT, Rondouin G. On the tracking of rapid dynamic changes in seizure EEG. IEEE Trans Biomed Eng 2002;39(9):952–8.
[16] Lea C, Flynn MD, Vidal R, Reiter A, Hager GD. Temporal convolutional networks for action segmentation and detection. In: 2017 IEEE conference on computer vision and pattern recognition. CVPR, 2017, p. 1003–12. http://dx.doi.org/10.1109/CVPR.2017.113.
[17] Ingolfsson TM, Hersche M, Wang X, Kobayashi N, Cavigelli L, Benini L. EEG-TCNet: An accurate temporal convolutional network for embedded motor-imagery brain–machine interfaces. In: 2020 IEEE international conference on systems, man, and cybernetics. SMC, 2020, p. 2958–65. http://dx.doi.org/10.1109/SMC42975.2020.9283028.
[18] Riyad M, Adib A. Investigation of attention based convolutional neural network for motor imagery classification. In: 2024 IEEE 12th international symposium on signal, image, video and communications. ISIVC, IEEE; 2024, p. 1–6.
[19] Ma X, Chen W, Pei Z, Zhang Y, Chen J. Attention-based convolutional neural network with multi-modal temporal information fusion for motor imagery EEG decoding. Comput Biol Med 2024;175:108504.
[20] Siino M, Bonomo G, Sorbello R, Tinnirello I. Investigating the impact of rational dilated wavelet transform on motor imagery EEG decoding with deep learning models. IEEE Access 2025;1. http://dx.doi.org/10.1109/ACCESS.2025.3645762.
[21] Schirrmeister RT, Springenberg JT, Fiederer LDJ, Glasstetter M, Eggensperger K, Tangermann M, Hutter F, Burgard W, Ball T. Deep learning with convolutional neural networks for EEG decoding and visualization. Hum Brain Mapp 2017;38(11):5391–420.
[22] Brunner C, Leeb R, Müller-Putz G, Schlögl A, Pfurtscheller G. BCI competition 2008–Graz data set A. Inst Knowl Discov (Lab Brain-Comput Interfaces) Graz Univ Technol 2008;16(1–6):1.
[23] Leeb R, Brunner C, Müller-Putz G, Schlögl A, Pfurtscheller G. BCI competition 2008–Graz data set B. Graz Univ Technol Austria 2008;16:1–6.
[24] Diwakar M, Singh P, Ravi V, Maurya A. A non-conventional review on multi-modality-based medical image fusion. Diagnostics 2023;13(5):820. http://dx.doi.org/10.3390/diagnostics13050820.
[25] Jindal M, Bajal E, Chakraborty A, Singh P, Diwakar M, Kumar N. A novel multi-focus image fusion paradigm: A hybrid approach. Mater Today: Proc 2021;37:2952–8. http://dx.doi.org/10.1016/j.matpr.2020.08.704.
[26] Zhou Y, Wang S, Chen Z, Yang H, Li L. Wavelet transform time–frequency image and convolutional neural network for motor imagery EEG classification. Sensors 2020;20(9):2514.
[27] Bashivan P, Rish I, Yeasin M, Codella N. Learning representations from EEG with deep recurrent-convolutional neural networks. In: International conference on learning representations. ICLR, 2016, p. N/A.
[28] Bayram I, Selesnick IW. Frequency-domain design of overcomplete rational-dilation wavelet transforms. IEEE Trans Signal Process 2009;57(8):2957–72.
[29] Lawhern VJ, Solon AJ, Waytowich NR, Gordon C, Hung C, Lance BJ. EEGNet: A compact convolutional neural network for EEG-based brain–computer interfaces. J Neural Eng 2018;15(5):056013.
[30] Wang T, Dong E, Du S, Jia C. A shallow convolutional neural network for classifying MI-EEG. In: 2019 Chinese automation congress. CAC, IEEE; 2019, p. 5837–41.
[31] Altuwaijri GA, Muhammad G, Altaheri H, Alsulaiman M. A multi-branch convolutional neural network with squeeze-and-excitation attention blocks for EEG-based motor imagery signals classification. Diagnostics 2022;12(4):995.
[32] Altaheri H, Muhammad G, Alsulaiman M. Physics-informed attention temporal convolutional network for EEG-based motor imagery classification. IEEE Trans Ind Inform 2022;19(2):2249–58.
[33] Thanarajan T, Rajendran S, et al. Sensor based EEG signal based dementia disease detection using artificial intelligence. J New Mater Electrochem Syst 2024;27(4).
[34] Balasubramani J, Surendran R. Explainable dense quantum recurrent model with Chebyshev swift flight optimization for autism classification using EEG signal. In: 2026 international conference on machine learning and autonomous systems. ICMLAS, IEEE; 2026, p. 1591–8.
[35] Pillai BS, Kulkarni R, kumar Kondeti VSS, Rajendran S. Wavelet transform-based bayesian inference learning with conditional variational autoencoder for mitigating injection attack in 6g edge network. Comput Model Eng Sci 2025;145(1):1141.
[36] Vaswani A, Shazeer N, Parmar N, Uszkoreit J, Jones L, Gomez AN, Kaiser L, Polosukhin I. Attention is all you need. In: Advances in neural information processing systems. vol. 30, 2017, p. 5998–6008.
[37] Schalk G, McFarland DJ, Hinterberger T, Birbaumer N, Wolpaw JR. BCI2000: A general-purpose brain-computer interface (BCI) system. In: IEEE transactions on biomedical engineering. vol. 51, IEEE; 2004, p. 1034–43.
[38] Cohen J. A coefficient of agreement for nominal scales. Educ Psychol Meas 1960;20(1):37–46. http://dx.doi.org/10.1177/001316446002000104, arXiv:https://doi.org/10.1177/001316446002000104.
[39] Huang X, Li Y, Chen Y, Lin Y, Yao D. An intelligent EEG classification methodology based on sparse representation enhanced deep learning networks. Front Neurosci 2020;14:808. http://dx.doi.org/10.3389/fnins.2020.00808, URL https://www.frontiersin.org/articles/10.3389/fnins.2020.00808/full.
[40] Opitz J. A closer look at classification evaluation metrics and a critical reflection of common evaluation practice. Trans Assoc Comput Linguist 2024;12:820–36. http://dx.doi.org/10.1162/tacl_a_00675, arXiv:https://direct.mit.edu/tacl/article-pdf/doi/10.1162/tacl_a_00675/2465598/tacl_a_00675.pdf.
[41] Wang T, Dong E, Du S, Jia C. A shallow convolutional neural network for classifying MI-EEG. In: 2019 Chinese automation congress. CAC, 2019, p. 5837–41.
[42] Altuwaijri GA, Muhammad G, Altaheri H, Alsulaiman M. A multi-branch convolutional neural network with squeeze-and-excitation attention blocks for EEG-based motor imagery signals classification. Diagnostics 2022;12(4):995.
[43] Altaheri H, Muhammad G, Alsulaiman M, Amin SU, Altuwaijri GA, Abdul W, Bencherif MA, Faisal M. Deep learning techniques for classification of electroencephalogram (EEG) motor imagery (MI) signals: A review. Neural Comput Appl 2023;35(20):14681–722.
[44] Li M-A, Han J-F, Duan L-J. A novel MI-EEG imaging with the location information of electrodes. IEEE Access 2019;8:3197–211.